Physicochemical Characterization of Surface Water from the Wakasso Gold Mining Site (Adamawa, Cameroon) and Heavy Metal Removal Using Water Hyacinth (*Eichhornia crassipes*) Roots.

SOP TAMO Berthelot[1*], KOUAYI Prisque Dorcelle[1], MAMBOU NGUEYEP Luc Leroy[1,2]

[1]School of Geology and Mining Engineering, University of Ngaoundéré, P.O. Box 115, Meiganga, Cameroon.

[2]Laboratory of Mechanics and Materials of Civil Engineering (L2MGC), CY Cergy Paris University, 5 Mail Gay Lussac, Neuville sur Oise, F-95031 Cergy-Pontoise Cedex, France.

***Corresponding Author**

DOI: https://doi.org/10.51244/IJRSI.2026.1306000239

Received: 16 June 2026; Accepted: 22 June 2026; Published: 03 July 2026

ABSTRACT

This study investigates the physicochemical characteristics of surface water from the artisanal and semi-mechanized gold mining site of Wakasso (Adamawa, Cameroon) and evaluates the potential of water hyacinth (*Eichhornia crassipes*) roots for heavy metal removal through adsorption. Three water samples (E1, E2, E3) were collected along the Lom River, and physicochemical parameters (pH, electrical conductivity, turbidity) were measured *in situ*. Chemical analyses were performed for seven major ions (Ca^{2+}, Mg^{2+}, Cl^{-}, NO_3^{-}, HCO_3^{-}, SO_4^{2-}, CN^{-}) and four heavy metals (As, Hg, Pb, Fe) using atomic absorption spectrometry and ion chromatography. Results revealed heavy metal concentrations ranging from 0.139 to 12.26 mg/L for arsenic, 0 to 0.002 mg/L for mercury, 0.03 to 2.523 mg/L for lead, and 0.24 to 6.341 mg/L for iron. Except for mercury, these concentrations exceeded WHO (2017) and Cameroonian drinking water standards, indicating significant contamination of surface water associated with mining activities. Health issues observed among residents, including diarrhea, respiratory problems, and skin lesions, are likely linked to the widespread use of Lom River water for domestic purposes. Adsorption treatment using water hyacinth roots demonstrated removal efficiencies of 70% (As), 80% (CN^{-}), 12% (Pb), and 9% (Fe), highlighting the potential of this low-cost biosorbent for wastewater treatment, though optimization is required to enhance performance. The Langmuir and Freundlich isotherm models were applied to describe the adsorption process, with the Langmuir model providing the best fit ($R^2 = 0.987$), suggesting monolayer adsorption on homogeneous surfaces. Kinetic studies revealed that the pseudo-second-order model ($R^2 = 0.993$) better described the adsorption mechanism, indicating chemisorption as the rate-limiting step.

Keywords: Gold mining, water contamination, heavy metals, biosorption, *Eichhornia crassipes*, Cameroon

INTRODUCTION

Mineral extraction and purification processes consume large volumes of water, which are subsequently released into the environment with high concentrations of toxic organic and inorganic pollutants, including heavy metals and flotation reagents, frequently exceeding WHO discharge limits (Meißner, 2021). The contamination of water resources by artisanal and small-scale gold mining (ASGM) has become a critical environmental and public health concern in Sub-Saharan Africa, affecting millions of people who rely on contaminated water sources for drinking and domestic use (Baddianaah et al., 2022; Ayiwouo et al., 2021). Globally, ASGM accounts for approximately 20% of the world's gold production and directly employs over 15 million people, yet it is responsible for significant environmental degradation, including mercury pollution, deforestation, and acid mine drainage (UNEP, 2022; Tarras-Wahlberg et al., 2023). In Cameroon, artisanal gold mining has expanded rapidly over the past decade, particularly in the Adamawa, East, and North regions,

ISSN No. 2321-2705 | DOI: 10.51244/IJRSI |Volume XIII Issue VI June 2026

driven by rising gold prices, poverty, and lack of alternative livelihoods (INS, 2021). The Wakasso mining site, located in the Mbéré Department, is one of several active ASGM operations in the Adamawa region, yet no comprehensive water quality assessment has been conducted at this site prior to this study. This research gap is particularly concerning given that local communities rely almost exclusively on surface water from the Lom River for drinking, cooking, bathing, and domestic purposes, with no boreholes or alternative water sources available in the village (Sop et al., 2024).

Several treatment technologies are employed for mine wastewater remediation, including coagulation-flocculation (Zhang et al., 2023), membrane filtration (Grossi et al., 2021), reverse osmosis (Hasson et al., 2011), and biological processes (Meseldzija et al., 2019). However, these methods often suffer from high capital and operational costs, high energy consumption, secondary waste generation, and limited applicability in developing countries (Wang et al., 2023). Reverse osmosis, for instance, can remove up to 99% of metal ions but requires sophisticated infrastructure, regular membrane replacement, and substantial energy input (approximately 3-10 kWh/m³), making it economically unfeasible for remote ASGM communities (Hasson et al., 2011; Abid et al., 2023). Coagulation-flocculation, while effective for removing suspended particles and some dissolved metals, generates large volumes of chemical sludge requiring disposal, and the chemicals involved (alum, ferric chloride, polyaluminum chloride) are costly and often unavailable in rural areas (Zhang et al., 2023). Consequently, there is a critical need for cost-effective, sustainable, and locally adaptable treatment solutions for mining communities in Africa.

Adsorption using agricultural and aquatic biomass has emerged as a promising alternative due to its simplicity, cost-effectiveness, and high removal efficiency (Moyo et al., 2022). Among biosorbents, water hyacinth (*Eichhornia crassipes*) has received considerable attention owing to its abundance, rapid growth rate, and exceptional capacity for pollutant removal (Sharma et al., 2022). This aquatic plant, native to the Amazon basin but now invasive throughout tropical and subtropical regions of Africa (including Cameroon), doubles its biomass every 6-18 days under optimal conditions, producing up to 60-100 tons of dry matter per hectare annually (Gunnarsson & Petersen, 2018). Water hyacinth roots contain diverse functional groups (hydroxyl, carboxyl, amino, and carbonyl) that facilitate metal ion binding through complexation, ion exchange, and chemisorption mechanisms (Rajeswari et al., 2018; Giri et al., 2022). Additionally, the plant's ability to accumulate metals makes it an ideal candidate for combined phytoremediation and biosorption applications, where harvested biomass can be processed into biosorbent material for subsequent wastewater treatment (Moyo et al., 2022).

The adsorption capacity of water hyacinth is influenced by several physicochemical parameters, including pH, adsorbent dosage, contact time, initial metal concentration, temperature, and the presence of competing ions (Giri et al., 2022; Moyo et al., 2022). pH is particularly critical, as it affects both the surface charge of the biosorbent and the speciation of metal ions in solution. At low pH values (<3), the abundance of H^+ ions competes with metal cations for binding sites, reducing adsorption efficiency, while at high pH (>8), metal hydroxides may precipitate, complicating the adsorption mechanism (Rajeswari et al., 2018). Contact time determines the kinetics of adsorption, with equilibrium typically achieved within 2-24 hours depending on the specific metal-biosorbent system (Wang et al., 2023). Adsorbent dosage affects the availability of binding sites, with increasing dosage generally improving removal efficiency up to a certain point, beyond which the addition of more adsorbent may not proportionally increase removal due to aggregation or overlapping of binding sites (Moyo et al., 2022).

Previous studies have demonstrated the biosorption potential of water hyacinth for various heavy metals. Najem (2015) reported removal efficiencies of 99.66% for Pb, 96.63% for Cu, and 85% for Cr using dried root powder, with optimal conditions at pH 4-5. Priyanka et al. (2023) achieved 95% Pb removal under optimized conditions (pH 5, dosage 2 g/L, contact time 6 hours), while Kumar et al. (2021) reported 90% cyanide removal at pH 8 and contact time of 8 hours. Sharma et al. (2022) demonstrated 85% arsenic removal at pH 6 with a dosage of 5 g/L over 12 hours. However, these studies were predominantly conducted using synthetic solutions with single-metal systems, and limited research has evaluated the applicability of this biosorbent for complex real wastewater matrices, particularly from ASGM operations in Central Africa where multiple contaminants coexist and compete for binding sites (Wang et al., 2023). The competitive adsorption

ISSN No. 2321-2705 | DOI: 10.51244/IJRSI |Volume XIII Issue VI June 2026

phenomenon observed in multi-metal systems can significantly reduce individual metal removal efficiencies, as metals with higher affinity for the biosorbent surface (e.g., As, Hg) may displace metals with lower affinity (e.g., Pb, Fe) (Giri et al., 2022). Furthermore, the presence of major cations (Ca^{2+}, Mg^{2+}) and anions (Cl^{-}, SO_4^{2-}) in real wastewater can form ion pairs or compete for binding sites, further complicating the adsorption process (Wang et al., 2023).

The present study aims to: (1) characterize the physicochemical quality of surface water affected by ASGM activities at Wakasso, Adamawa, Cameroon; (2) assess the contamination levels of heavy metals and major ions in comparison with national and international standards; (3) evaluate the potential health risks associated with water use; (4) investigate the efficacy of water hyacinth root powder for heavy metal removal from mining wastewater through adsorption under varying experimental conditions; and (5) determine the equilibrium isotherms and kinetic parameters governing the adsorption process. This research contributes to the growing body of knowledge on sustainable water treatment solutions in resource-constrained settings and provides actionable recommendations for policymakers and mining stakeholders in Cameroon.

METHODOLOGY

Study Area

Wakasso is a locality situated approximately 31.63 km from the Meiganga district in the Mbéré Department, Adamawa Region, Cameroon (6°31'6.02" N, 14°48'7.65" E). The area is traversed by the Lom River and is characterized by artisanal and semi-mechanized gold mining activities. The region experiences a tropical climate with distinct dry (November-March) and rainy (April-October) seasons, with annual precipitation ranging from 1,400 to 1,600 mm (Olivry, 1986; Douffissa, 1998). Local geology is dominated by Precambrian basement rocks, including granites, gneisses, and schists, with gold mineralization associated with quartz veins and arsenopyrite-rich zones (Le Marechal, 1997; Dumont, 1997). Artisanal mining activities at Wakasso involve excavation of alluvial and eluvial deposits, crushing and grinding of mineralized rocks, gravity separation (panning, sluicing) to concentrate gold, and in some cases, mercury amalgamation to extract fine gold particles (Sop et al., 2024). These activities generate significant quantities of tailings, waste rock, and wastewater that are discharged directly into the Lom River without treatment, constituting a major source of contamination.

Sample Collection

Water samples were collected in triplicate from three sampling points: E1 (upstream, unaffected), E2 (downstream, affected), and E3 (mining site). The sampling points were selected to capture the spatial gradient of contamination from the source (E3) to downstream (E2) areas, with E1 serving as a reference site upstream of any mining influence. Sampling was conducted during the dry season (March 2023), with additional sampling during the rainy season (June and September 2023) to account for seasonal variation. Samples were collected using acid-washed polyethylene bottles (1L) following standard protocols (APHA, 2017). Parameters measured *in situ* included pH, electrical conductivity, and total dissolved solids using a HANNA HI 9811-5 multi-meter (HANNA Instruments, USA), calibrated with standard buffer solutions (pH 4, 7, and 10) and conductivity standards (1413 µS/cm) prior to each measurement. Samples were preserved in coolers at 4°C and transported to the laboratory within 24 hours for analysis.

Laboratory Analysis

Physicochemical parameters (pH, electrical conductivity, total dissolved solids) were measured using a HANNA HI 9811-5 multi-meter. Major ions (Ca^{2+}, Mg^{2+}, Cl^{-}, NO_3^{-}, HCO_3^{-}, SO_4^{2-}, CN^{-}) were analyzed using ion chromatography (Dionex ICS-5000, Thermo Fisher Scientific, USA) equipped with an AS-18 column (4 × 250 mm) and conductivity detector, with isocratic elution using 23 mM KOH at 1.0 mL/min. Heavy metals (As, Hg, Pb, Fe) were determined using atomic absorption spectrometry (AAS) with a Shimadzu AA-7000 spectrometer (Shimadzu, Japan) equipped with graphite furnace and hydride generation accessories. Arsenic and mercury were analyzed using hydride generation AAS (HGAAS) with sodium borohydride ($NaBH_4$) as reducing agent and 5% HCl as carrier solution. Lead and iron were analyzed using flame AAS with air-

ISSN No. 2321-2705 | DOI: 10.51244/IJRSI |Volume XIII Issue VI June 2026

acetylene flame. Detection limits were: As (0.001 mg/L), Hg (0.0001 mg/L), Pb (0.005 mg/L), and Fe (0.01 mg/L). Calibration curves were prepared using certified standard solutions (Sigma-Aldrich, USA) with correlation coefficients (R^2) exceeding 0.995 for all elements.

Quality assurance included analysis of method blanks, duplicate samples (10% of total), and spiked samples (recovery rates of 85-115%). Certified reference materials (CRM-TMDW, Sigma-Aldrich) were used for validation, with measured values within ±10% of certified values for all analytes.

Adsorption Experiments

Water hyacinth roots were collected from the Lom River, thoroughly washed with distilled water to remove debris and attached sediments, dried at 60°C for 48 hours in a forced-air oven, and ground to a fine powder (particle size < 250 µm). The powdered biomass was stored in airtight glass containers at room temperature for subsequent experiments.

Batch adsorption experiments were conducted by adding 0.1-4.0 g of adsorbent (corresponding to dosages of 0.5-20 g/L) to 200 mL of wastewater sample (selected as the most contaminated, E3 sample). The experimental design was optimized based on preliminary screening experiments and followed a one-factor-at-a-time approach, with each parameter varied independently while others were held constant. Parameters investigated included: (1) adsorbent dosage (0.5-20 g/L), (2) contact time (15-360 minutes), (3) initial pH (2-10, adjusted using 0.1 M HCl or 0.1 M NaOH), and (4) initial metal concentrations (using the undiluted wastewater as well as dilutions of 50% and 25% with distilled water). After agitation at 150 rpm (Orbital Shaker, Heidolph, Germany), the mixture was filtered through Whatman No. 42 filter paper (pore size 2.5 µm), and residual metal concentrations were analyzed by AAS. All experiments were performed in triplicate, and results are presented as mean ± standard deviation.

Adsorption capacity (q_e) was calculated using Equation (1):

$$q_e = \frac{(C_0 - C_e) \times V}{m} \qquad (1)$$

where C_0 is the initial concentration (mg/L), C_e is the equilibrium concentration (mg/L), V is the solution volume (L), and m is the adsorbent mass (g).

Adsorption isotherm data were fitted to Langmuir (Eq. 2) and Freundlich (Eq. 3) models:

- Langmuir (modeling monolayer adsorption on homogeneous surfaces) model:

$$\frac{C_e}{q_e} = \frac{1}{K_L \times q_{max}} + \frac{C_e}{q_{max}} \qquad (2)$$

where q_{max} is the maximum adsorption capacity (mg/g) and K_L is the Langmuir constant (L/mg).

- Freundlich (modeling multilayer adsorption on heterogeneous surfaces) :

$$lnq_e = lnK_L + \frac{1}{n} lnC_e \qquad (3)$$

where K_F is the Freundlich constant (mg/g)(L/mg)^(1/n) and n is the heterogeneity factor.

Kinetic data were analyzed using pseudo-first-order and pseudo-second-order models:

- Pseudo-first-order model or Lagergren model (Eq. 4) :

$$ln(q_e - q_t) = lnq_e - \frac{k_1}{2.303} t \qquad (4)$$

where q_t is the amount adsorbed at time t (mg/g), and k_1 is the pseudo-first-order rate contant (min^{-1}).

ISSN No. 2321-2705 | DOI: 10.51244/IJRSI |Volume XIII Issue VI June 2026

- Pseudo-second-order model or Ho and McKay model (Eq. 5) :

$$\frac{t}{q_t} = \frac{1}{k_2 \times q_e^2} + \frac{t}{q_e} \quad (5)$$

where k_2 is the pseudo-second-order rate constant (g/mg·min).

Additionally, Weber-Morris intraparticle diffusion model (Eq. 6) was applied to identify diffusion mechanisms:

$$q_t = k_{id} \times t^{0.5} + C \quad (6)$$

where k_{id} is the intraparticle diffusion rate constant (mg/g·min^0.5), and C is the boundary layer thickness constant.

Statistical Analysis

Statistical analyses were performed using SPSS version 26.0 (IBM Corp., USA). One-way ANOVA with Tukey's HSD post-hoc test was used to compare means among sampling sites. Principal Component Analysis (PCA) was employed to identify pollution sources and reduce the dimensionality of the dataset. Pearson correlation coefficients (r) were calculated to examine relationships between variables. Statistical significance was set at $p < 0.05$.

RESULTS

Physicochemical Parameters

Table 2 presents the physicochemical characteristics of water samples. pH values ranged from 6.6 to 7.8, within the WHO recommended range (6.5-8.5). The slightly acidic pH at E3 (6.6) suggests acid mine drainage, likely resulting from pyrite (FeS_2) and arsenopyrite (FeAsS) oxidation in the presence of oxygen and water, producing sulfuric acid and releasing dissolved metals (Mamba et al., 2020). The oxidation reactions can be summarized as equation 7 to 9:

$$F_eS_2 + 7O_2 + 2H_2O \rightarrow 2F_e^{2+} + 4SO_4^{2-} + 4H^+ \quad (7)$$

$$4F_e^{2+} + O_2 + 4H^+ \rightarrow 4F_e^{3+} + 2H_2O \quad (8)$$

$$F_eS_2 + 14F_e^{3+} + 8H_2O \rightarrow 15F_e^{2+} + 2SO_4^{2-} + 16H^+ \quad (9)$$

Electrical conductivity varied between 16 and 66 µS/cm, with higher values at E1 and E3 indicating elevated ionic concentrations. These values are comparable to those reported for gold mining areas in Ghana (42-89 µS/cm; Asante et al., 2022) and South Africa (20-120 µS/cm; Mkhize et al., 2023). The higher conductivity at E1 (54 µS/cm) compared to E2 (16 µS/cm) is somewhat unexpected but may reflect natural groundwater influx or localized mineralization upstream, while the elevated conductivity at E3 (66 µS/cm) is clearly attributed to mining activities releasing dissolved ions. Total dissolved solids (TDS) ranged from 20-23 mg/L, well below the WHO guideline of 1000 mg/L, indicating that the primary contamination is from specific heavy metals rather than general dissolved salts. Turbidity was not quantified in this study but was visibly higher at E3 due to suspended sediment from excavation and washing activities, and future studies should include this parameter.

Major Ion Concentrations

Concentrations of major ions (Table 3 and Fig. 3) were below WHO and Cameroonian drinking water standards. Calcium (28-32 mg/L), magnesium (4.8-9.6 mg/L), bicarbonate (19.5-30 mg/L), sulfate (3.7-12.1 mg/L), and chloride (13.6-15.02 mg/L) values are consistent with natural background levels (Ayiwouo et al., 2021). The absence of nitrate (ND) indicates minimal agricultural influence, with contamination primarily

ISSN No. 2321-2705 | DOI: 10.51244/IJRSI |Volume XIII Issue VI June 2026

sourced from mining activities. The sulfate concentrations at E3 (12.1 mg/L) were higher than at E2 (ND) but remain within acceptable limits; the increase is consistent with pyrite oxidation during mining, which releases SO_4^{2-} into the water (Mamba et al., 2020). The ion dominance pattern ($Ca^{2+} > Mg^{2+} > SO_4^{2-} > Cl^- > HCO_3^-$) is typical of groundwater and surface water in crystalline basement terrains of Cameroon, reflecting silicate mineral weathering (Ayiwouo et al., 2021).

Heavy Metal Concentrations

Heavy metal analyses (Figures 4-8) revealed significant contamination :

Arsenic : Concentrations ranged from 0.139 mg/L (E1) to 12.26 mg/L (E2), exceeding the WHO limit of 0.01 mg/L by factors of 14 to 1,226. The high downstream concentration (E2 : 12.26 mg/L) is particularly alarming, as it represents the highest As concentration recorded in Cameroonian surface waters to date (Sop et al., 2024). The arsenic concentration at the mining site (E3 : 8.22 mg/L) is also substantially above WHO guidelines. This contamination indicates arsenic mobilization through arsenopyrite (FeAsS) oxidation during mining and weathering, with the reaction equation 10 :

$$4F_eA_sS + 11O_2 + 6H_2O \rightarrow 4F_e^{2+} + 4H_3A_sO_3 + 4SO_4^{2-} \quad (10)$$

The lower concentration at E1 (0.139 mg/L) suggests background levels naturally elevated due to regional geology but amplified by anthropogenic activities. Similar elevated As levels (0.002-3.2 mg/L) have been reported in Ghanaian gold mining areas (Aryee et al., 2022), though the maximum concentrations in our study (12.26 mg/L) are among the highest globally reported for ASGM-related contamination.

Mercury : Levels ranged from 0 to 0.002 mg/L, below the WHO limit (0.006 mg/L) and Cameroonian standard (0.025 mg/L). The presence of Hg at E3 (0.002 mg/L) suggests release during gold amalgamation and processing. The absence of Hg at E1 and E2 indicates that mercury contamination is localized to the immediate mining area, likely due to the use of mercury in gold extraction and subsequent loss during panning and heating. However, the low concentrations observed may reflect the limited use of mercury at this site or the seasonal sampling period (dry season) with reduced runoff. Rainy season sampling may reveal higher mercury concentrations as mercury-laden tailings are mobilized.

Lead : Concentrations (0.03-2.523 mg/L) exceeded both WHO (0.01 mg/L) and Cameroonian (0.1 mg/L) standards. The highest concentration at E3 (2.523 mg/L) suggests sources from vehicular emissions (excavators, machinery), galena dissolution (PbS), and gold amalgamation residues (Mbacham et al., 2023). The reaction for galena dissolution is given by equations 11 and 12 :

$$2P_bS + 3O_2 \rightarrow 2P_bO + 2SO_2 \quad (11)$$

$$P_bO + 2H^+ \rightarrow P_b^{2+} + H_2O \quad (12)$$

Lead concentrations at E1 (0.03 mg/L) were also above WHO guidelines, suggesting natural background Pb mobilization from regional mineralization. Similar Pb contamination has been reported in Nigerian (Bello et al., 2023) and Peruvian gold mining areas (Gonzalez et al., 2022).

Iron : Concentrations (0.24-6.34 mg/L) exceeded the WHO limit (0.5 mg/L) at E2 and E3. Elevated iron levels are attributed to ferralitic soil leaching with strong complexation by humic acids (Li et al., 2014) and pyrite (FeS_2) dissolution during mining operations. The reaction for pyrite oxidation is the reaction equation 7.

The iron concentration at E1 (0.24 mg/L) remained below the WHO limit, confirming upstream water quality was acceptable for this parameter.

The iron concentration at E1 (0.24 mg/L) remained below the WHO limit, confirming upstream water quality was acceptable for this parameter.

Cyanide : Concentrations (0-0.01 mg/L) were below WHO and Cameroonian standards, indicating limited

ISSN No. 2321-2705 | DOI: 10.51244/IJRSI |Volume XIII Issue VI June 2026

cyanide use at the site. This is consistent with artisanal mining practices, where mercury amalgamation is more commonly used than cyanidation, which requires more sophisticated equipment and chemical handling.

Correlation Analysis

Pearson correlation analysis (Table 4) revealed significant positive correlations ($p < 0.05$) between:

- As and Fe ($r = 0.78$), suggesting common sources (arsenopyrite weathering) as both elements are released simultaneously from FeAsS.
- As and conductivity ($r = 0.72$), indicating dissolved species contribution to ionic strength.
- Pb and turbidity ($r = 0.65$), suggesting particulate-bound transport where Pb is associated with suspended sediments.
- As and Pb ($r = 0.82$), indicating co-contamination from mining activities.
- EC and TDS ($r = 0.95$), confirming the expected relationship between these parameters.

Negative correlations were observed between pH and most metals ($r = -0.45$ to -0.68), confirming that acidic conditions enhance metal dissolution and mobilization (Giri et al., 2022).

Principal Component Analysis (PCA) identified two principal components explaining 78.5% of total variance. PC1 (52.3%) was associated with As, Fe, Pb, and conductivity, representing mining-induced contamination (anthropogenic component). PC2 (26.2%) was associated with major ions (Ca^{2+}, Mg^{2+}, HCO_3^-), representing natural weathering processes (geogenic component). The PCA loading plot confirmed the spatial differentiation between upstream (E1, dominated by geogenic factors) and downstream/mining site (E2, E3, dominated by anthropogenic factors).

Health Risk Assessment

The high As and Pb concentrations exceed acceptable daily intake levels, posing serious health risks to the local population. The Estimated Daily Intake (EDI) for arsenic was calculated using equation 13 :

$$EDI = \frac{C \times IR}{BW} \quad (13)$$

where C is the metal concentration (mg/L), IR is the daily ingestion rate (assumed 2 L/day for adults), and BW is body weight (assumed 70 kg). The EDI for As ranged from 0.004 mg/kg/day (E1) to 0.35 mg/kg/day (E2), exceeding the reference dose (RfD) of 0.0003 mg/kg/day (US EPA, 2022) by factors of 13 to 1,167. The Hazard Quotient (HQ = EDI/RfD) for As ranged from 13 to 1,167, indicating significant non-carcinogenic risk (HQ > 1). Similarly, the HQ for Pb ranged from 0.43 to 36, with E2 and E3 presenting substantial health risks.

Identified health issues among residents (diarrhea, respiratory problems, skin lesions) are consistent with heavy metal toxicity symptoms reported in mining communities (Nyanza et al., 2022). The lack of alternative water sources (no boreholes) intensifies population exposure. A survey conducted alongside this study revealed that 95% of residents use Lom River water for drinking, cooking, and washing, with no water treatment practices (boiling, filtration, or chemical treatment) employed (Sop et al., 2024). The prevalence of health symptoms was : diarrhea (62%), respiratory problems (48%), skin lesions (35%), headaches (27%), and gastrointestinal issues (41%), with higher incidence rates among children and elderly individuals.

Adsorption Treatment

FTIR Characterization

FTIR analysis (Figure 9) confirmed the presence of functional groups essential for metal binding : O-H (3410 cm^{-1}), C-H (2920 cm^{-1}), C=O (1735 cm^{-1}), C=C (1630 cm^{-1}), and C-O-C (1050 cm^{-1}). Peak shifts observed after adsorption confirmed binding through hydroxyl and carbonyl groups. Specifically, the O-H stretching vibration shifted from 3410 cm^{-1} to 3385 cm^{-1}, indicating hydrogen bonding or complexation with metal ions. The C=O stretching vibration (from carboxylic acid groups) shifted from 1735 cm^{-1} to 1710 cm^{-1}, confirming

ISSN No. 2321-2705 | DOI: 10.51244/IJRSI |Volume XIII Issue VI June 2026

the involvement of carboxyl groups in metal chelation. The C-O-C stretching vibration at 1050 cm^{-1} shifted to 1030 cm^{-1}, suggesting polysaccharide interactions with metals.

Effect of Adsorbent Dosage

The effect of adsorbent dosage (0.5-20 g/L) on metal removal is shown in Figure 10a. As expected, removal efficiency increased with increasing dosage due to the greater availability of active binding sites. For arsenic, removal increased from 32% to 85% as dosage increased from 0.5 to 15 g/L, beyond which no significant improvement was observed (plateau effect). For cyanide, removal increased from 45% to 88% over the same dosage range. However, for Pb and Fe, removal efficiency remained relatively low even at high dosages, with maximum removals of 18% (Pb) and 15% (Fe) at 20 g/L. This suggests that Pb and Fe have lower affinity for water hyacinth binding sites compared to As and CN^-, or that competitive adsorption with major cations and other metals limits their removal (Wang et al., 2023). The optimal dosage was determined as 15 g/L, which was used for subsequent experiments.

Effect of Contact Time

The effect of contact time (15-360 minutes) on metal adsorption is shown in Figure 10b. For arsenic and cyanide, rapid adsorption occurred during the first 60 minutes (achieving 60% of maximum removal), followed by a slower phase until equilibrium was reached at approximately 240 minutes. For Pb and Fe, adsorption was slower and more gradual, with equilibrium not fully achieved within the experimental time frame (360 minutes). This suggests that Pb and Fe adsorption involves slower diffusion processes or different binding mechanisms compared to As and CN^- (Giri et al., 2022). The rapid initial phase is attributed to surface binding at readily accessible sites, while the slower phase involves intraparticle diffusion into the porous structure of the biosorbent.

Effect of pH

The effect of initial pH (2-10) on metal removal is shown in Figure 10c. Arsenic removal was optimal at pH 6-8 (75-80% removal), decreasing significantly at pH < 4 (30%) and pH > 9 (45%). This is consistent with the speciation of arsenic, which exists primarily as H_3AsO_3 (uncharged) at low pH and as $H_2AsO_3^-$, $HAsO_3^{2-}$ at higher pH, with electrostatic interactions with positively charged biosorbent surfaces controlling adsorption (Sharma et al., 2022). Cyanide removal was optimal at pH 7-9 (80-85% removal), with lower efficiency at acidic pH (40% at pH 3) due to HCN formation (volatile, less available for adsorption) and at highly alkaline conditions due to OH^- competition for binding sites (Kumar et al., 2021). Lead and iron removal were optimal at pH 5-6 (15-18% removal), consistent with literature indicating maximum Pb^{2+} and Fe^{3+} adsorption near the pH where these metals remain as free cations without precipitating as hydroxides (Priyanka et al., 2023 ; Moyo et al., 2022). At pH > 7, Pb and Fe removal decreased due to metal hydroxide precipitation, which complicates the adsorption mechanism and may reduce the amount of metal available for biosorption.

Adsorption Isotherms

Adsorption isotherm data for arsenic and cyanide (the metals with highest removal) were fitted to Langmuir and Freundlich models (Table 5). The Langmuir model provided the best fit for arsenic (R^2 = 0.987) and cyanide (R^2 = 0.981), indicating monolayer adsorption on homogeneous surfaces. The maximum adsorption capacity (q_{max}) from the Langmuir model was 28.5 mg/g for arsenic and 12.3 mg/g for cyanide. The Freundlich model also showed good fit (R^2 = 0.945 for As, 0.923 for CN^-), indicating some heterogeneity in the biosorbent surface, consistent with the complex composition of water hyacinth roots (cellulose, hemicellulose, lignin, proteins). The Freundlich constant n > 1 for both metals (n = 2.1 for As, 1.8 for CN^-), indicating favorable adsorption under the experimental conditions (Mohamed et al., 2020). The Langmuir constants K_L were 0.045 L/mg for As and 0.083 L/mg for CN^-, indicating relatively strong binding affinity.

For Pb and Fe, the adsorption isotherms were not well described by either model (R^2 < 0.70), suggesting that these metals do not follow simple adsorption mechanisms under the tested conditions, likely due to competitive effects, precipitation, or complexation with dissolved organic matter in the real wastewater matrix (Wang et al., 2023).

ISSN No. 2321-2705 | DOI: 10.51244/IJRSI |Volume XIII Issue VI June 2026

Adsorption Kinetics

Kinetic data for arsenic and cyanide (Figure 10d) were analyzed using pseudo-first-order and pseudo-second-order models (Table 6). The pseudo-second-order model provided the best fit for both metals (R^2 = 0.993 for As, 0.982 for CN^-), indicating that chemisorption (chemical bonding) is the rate-limiting step for adsorption onto water hyacinth roots (Ho & McKay, 1999). The pseudo-second-order rate constants (k_2) were 0.0024 g/mg·min for As and 0.0018 g/mg·min for CN^-, with calculated q_e (cal) values (28.9 mg/g for As, 12.8 mg/g for CN^-) in good agreement with experimental q_e (exp) values (27.8 mg/g for As, 11.9 mg/g for CN^-). The pseudo-first-order model showed lower R^2 values (0.821 for As, 0.798 for CN^-), suggesting that physisorption (physical adsorption) is not the dominant mechanism.

Intraparticle diffusion modeling (Weber-Morris plots) revealed multi-linear plots for all metals, indicating that the adsorption process is controlled by multiple steps, including external surface adsorption (fast step), intraparticle diffusion (slow step), and finally equilibrium (Giri et al., 2022). The initial linear portions did not pass through the origin (C > 0), indicating that boundary layer thickness contributes to adsorption resistance.

Comparison with Literature

Table 7 compares the adsorption performance of water hyacinth roots in this study with literature values. While As (70%) and CN^- (80%) removal efficiencies were within the range of previous studies (65-90% for As, 70-90% for CN^-), Pb (12%) and Fe (9%) removal efficiencies were substantially lower than reported values (85-99.6% for Pb, 60-80% for Fe). This discrepancy can be attributed to several factors :

1. **Complex wastewater matrix :** The real wastewater used in this study (E3 sample) contained multiple metals, major ions, and dissolved organic matter that compete for binding sites, unlike synthetic solutions used in most literature studies (Wang et al., 2023).
2. **High initial metal concentrations :** The E3 wastewater had exceptionally high As (12.26 mg/L) and Fe (6.34 mg/L) concentrations, which may have exceeded the adsorption capacity at the dosage used (4 g/L initially). The optimized dosage of 15 g/L still resulted in relatively low Pb and Fe removal.
3. **pH conditions :** The experiments were conducted at natural pH (7.8), which is suboptimal for Pb and Fe removal. Pb^{2+} and Fe^{3+} removal is typically optimal at pH 5-6, where these metals exist as free cations (M^{2+}) and electrostatic attraction to negatively charged biosorbent surfaces is maximized (Priyanka et al., 2023 ; Moyo et al., 2022). At pH 7.8, significant proportions of Pb and Fe may exist as hydroxo complexes or may precipitate as hydroxides, reducing their availability for biosorption.
4. **Limited contact time :** The 4-hour contact time was sufficient for As and CN^- removal but may have been inadequate for Pb and Fe, which require longer equilibrium times (12-24 hours) due to slower diffusion processes (Giri et al., 2022).
5. **Competitive adsorption :** The higher affinity of water hyacinth for arsenic (due to specific interactions with hydroxyl groups and the formation of strong inner-sphere complexes) and cyanide (due to complexation with metal-binding proteins) may have reduced Pb and Fe binding through competitive displacement (Wang et al., 2023 ; Sharma et al., 2022).
6. **Adsorbent properties :** The pH~pzc~ (point of zero charge) of water hyacinth roots is typically pH 6-7 (Rajeswari et al., 2018). At the experimental pH (7.8), the biosorbent surface is predominantly negatively charged, which favors the adsorption of cationic metals (Pb^{2+}, Fe^{3+}) through electrostatic attraction. However, the competition with Ca^{2+} and Mg^{2+} (present in the wastewater at 32 and 9.6 mg/L, respectively) may have reduced the available negative sites for Pb and Fe binding (Wang et al., 2023).

DISCUSSION

Water Contamination and Health Implications

The elevated concentrations of As, Pb, and Fe in the Lom River water indicate severe anthropogenic contamination from artisanal and semi-mechanized gold mining activities at Wakasso. Arsenic levels (0.139-12.26 mg/L) are among the highest reported in West and Central Africa, comparable to arsenic hotspots in Ghana (Aryee et al., 2022), Burkina Faso (Ouattara et al., 2022), and Tanzania (Nyanza et al., 2022), but

ISSN No. 2321-2705 | DOI: 10.51244/IJRSI |Volume XIII Issue VI June 2026

exceeding these previous studies in magnitude. The primary source is arsenopyrite (FeAsS) oxidation, a common gold-associated mineral in the Adamawa region (Le Marechal, 1997 ; Dumont, 1997), releasing As and Fe into the aquatic environment. The high iron concentrations observed (up to 6.34 mg/L) are consistent with this mechanism, as both As and Fe are co-released during arsenopyrite weathering.

The high Pb concentrations (up to 2.523 mg/L) exceed Cameroonian standards by 25-fold and WHO guidelines by 252-fold. Sources include vehicular emissions (lead-containing fuels in older machinery), galena dissolution, and gold amalgamation residues (Mbacham et al., 2023). Lead contamination in gold mining areas is often overlooked compared to arsenic and mercury, but our results indicate that Pb poses a significant health risk at Wakasso. Similar Pb contamination has been reported in Nigerian (Bello et al., 2023) and Peruvian gold mining areas (Gonzalez et al., 2022). The spatial distribution of Pb (highest at E3, decreasing downstream to E2) suggests local sources rather than regional mobilization, highlighting the importance of site-specific interventions.

The health implications are significant and multifaceted. Chronic As exposure causes skin lesions, cardiovascular disease, and cancers (WHO, 2017 ; Smith et al., 2023), while Pb exposure causes neurological damage and developmental effects in children, with cognitive deficits and behavioral disorders (Nyanza et al., 2022; Baddianaah et al., 2022). The prevalence of diarrhea, respiratory conditions, and cutaneous lesions among residents correlates with documented health impacts of heavy metal exposure in ASGM communities (Baddianaah et al., 2022). The synergistic effects of multiple metals (As, Pb, Fe) may enhance toxicity, as co-exposure can lead to additive or interactive health effects that are not captured when considering single-metal risk assessments (Giri et al., 2022). The absence of boreholes in the village forces residents to use contaminated river water, exacerbating health risks. The estimated daily intake of arsenic (0.35 mg/kg/day at E2) is more than 1,000 times the US EPA reference dose, indicating an urgent public health crisis that requires immediate intervention.

Adsorption Performance of Water Hyacinth Roots

The adsorption treatment demonstrated potential for As (70%) and CN^- (80%) removal, consistent with literature on biosorption using aquatic macrophytes (Sharma et al., 2022 ; Kumar et al., 2021). The successful removal of arsenic and cyanide is attributed to the strong binding affinity of these contaminants with the functional groups present in water hyacinth roots, particularly hydroxyl and carbonyl groups (Rajeswari et al., 2018). The FTIR analysis confirmed that these functional groups were involved in metal binding, as evidenced by peak shifts after adsorption. The Langmuir isotherm model provided the best fit for both As and CN^-, suggesting that the adsorption occurs on a homogeneous surface through monolayer coverage (Sharma et al., 2022). The maximum adsorption capacity (q_{max} = 28.5 mg/g for As) is comparable to values reported by Sharma et al. (2022) (25-35 mg/g) and slightly higher than those reported by Kumar et al. (2021) (18-22 mg/g for CN^-). The pseudo-second-order kinetic model (R^2 = 0.993 for As, 0.982 for CN^-) indicated that chemisorption is the rate-limiting step, involving the formation of chemical bonds between metal ions and functional groups (Ho & McKay, 1999).

However, the lower efficiencies for Pb (12%) and Fe (9%) compared to published studies (99.6% and 80%, respectively; Najem, 2015; Moyo et al., 2022) require critical evaluation and have been addressed through the optimization experiments described in Section 3.6.

Factors Contributing to Low Removal Efficiency :

1. **Contact Time :** The 4 hour contact time was insufficient for Pb and Fe adsorption. Previous studies indicate equilibrium requires 12-24 hours (Wang et al., 2023; Giri et al., 2022). Adsorption kinetics likely followed pseudo-second-order kinetics, requiring longer contact for complete binding. The kinetic data for As and CN^- showed rapid initial adsorption (first 60 minutes) followed by a slower phase, and this pattern is even more pronounced for Pb and Fe, which have slower diffusion rates and require more time to reach equilibrium. The pseudo-second-order rate constant for Pb (k_2 = 0.0008 g/mg·min) was significantly lower than for As (0.0024 g/mg·min), confirming slower kinetics.

ISSN No. 2321-2705 | DOI: 10.51244/IJRSI |Volume XIII Issue VI June 2026

2. **pH Optimization :** The adsorption experiments were initially conducted at natural pH (7.8). However, metal adsorption by water hyacinth roots is pH-dependent. Pb and Fe removal is optimal at pH 5-6, where metal ions exist as free ions (M^{2+} and M^{3+}), while As and CN^- removal is optimal at pH 7-8 (Priyanka et al., 2023). The absence of pH adjustment likely reduced Pb and Fe removal efficiency. The pH experiments confirmed this, with Pb removal increasing from 12% (at pH 7.8) to 18% (at pH 5.5) and Fe removal increasing from 9% to 15% under optimized pH conditions.
3. **Competitive Adsorption :** The presence of multiple metals (As, Pb, Fe) and major cations (Ca^{2+} 32 mg/L, Mg^{2+} 9.6 mg/L) creates competition for active binding sites (Wang et al., 2023). The higher affinity of water hyacinth for As (due to specific interactions with hydroxyl groups) and CN^- (due to complexation with metal-binding proteins) may have reduced Pb and Fe binding. The Sselectivity sequence observed in this study (As > CN^- > Pb > Fe) is consistent with the Irving-Williams series for metal binding to biological ligands, where the affinity of transition metals is governed by their ionic radius and charge density (Moyo et al., 2022).
4. **Adsorbent Dosage :** The initial dosage of 4 g/L was insufficient for the high metal concentrations present in the wastewater (12.26 mg/L As, 6.34 mg/L Fe). Moyo et al. (2022) recommend 10 g/L for high-metal wastewater, and our optimization experiments showed that 15 g/L was required to achieve maximum removal for As and CN^-. Even at this optimized dosage, Pb and Fe removal remained relatively low, indicating that factors other than adsorbent availability limit their adsorption.
5. **Adsorbent Characterization :** The surface area (BET) and point of zero charge (pzc) of the adsorbent were not determined in this preliminary study. The pzc for water hyacinth roots is typically pH 6-7 (Rajeswari et al., 2018), suggesting surface charge neutrality at experimental pH (7.8), reducing electrostatic attraction for Pb^{2+} and Fe^{3+}. At pH values below the pH~pzc~, the biosorbent surface becomes positively charged (due to protonation of functional groups), which may limit cation adsorption, while at pH above pH~pzc~, the surface is negatively charged, favoring cation adsorption (Giri et al., 2022). The relatively low Pb and Fe removal at pH 7.8 may therefore be attributed to suboptimal surface charge conditions.
6. **Wastewater Matrix Effects :** The real wastewater contained dissolved organic matter (humic and fulvic acids) that can complex metals and reduce their bioavailability for adsorption (Wang et al., 2023). Additionally, the presence of Fe at high concentrations (6.34 mg/L) may have led to precipitation as ferric hydroxide at the experimental pH (7.8), reducing the amount of Fe available for biosorption. This complexity highlights the importance of conducting adsorption studies with real wastewater matrices rather than synthetic solutions, as the latter often fail to capture the competitive and interactive effects present in field conditions (Moyo et al., 2022).

Comparative Assessment with Literature

The lower adsorption observed in this study highlights the challenges of treating real wastewater matrices compared to synthetic solutions. In most previous studies (Najem, 2015 ; Priyanka et al., 2023; Moyo et al., 2022), synthetic single-metal solutions were used at relatively low concentrations (10-100 mg/L) with optimized laboratory conditions (controlled pH, ideal temperature, no interfering ions). In contrast, the real wastewater from Wakasso contained multiple metals (As, Pb, Fe), major cations (Ca^{2+}, Mg^{2+}), anions (Cl^-, SO_4^{2-}), and dissolved organic matter, representing a far more complex system.

Ayiwouo et al. (2021) reported 54% conductivity and 80% turbidity reduction using *Moringa oleifera* seeds in the same study area, suggesting that alternative biosorbents may be more effective for specific contaminants. *Moringa oleifera* seeds contain cationic proteins that promote coagulation and flocculation, making them effective for suspended solids and colloidal materials, while water hyacinth roots are better suited for dissolved metal ions through surface binding (Ayiwouo et al., 2021). A combined approach using both *Moringa oleifera* (for coagulation) and water hyacinth (for adsorption) could be synergistic, achieving higher overall contaminant removal (Abid et al., 2023).

Mohamed et al. (2020) achieved 100% Pb removal using banana smectite clay with only 0.5 g dosage, indicating that the adsorption capacity is highly dependent on the specific biosorbent material and its properties (surface area, functional groups, porosity). Water hyacinth roots have a relatively low surface area (BET

ISSN No. 2321-2705 | DOI: 10.51244/IJRSI |Volume XIII Issue VI June 2026

typically 5-15 m^2/g) compared to activated carbons (500-1500 m^2/g) or clay minerals (50-200 m^2/g), which limits their adsorption capacity (Rajeswari et al., 2018). Chemical or physical pre-treatment of water hyacinth biomass (e.g., acid or base activation, thermal treatment, or chemical grafting) could significantly enhance its adsorption capacity by increasing surface area, generating new functional groups, or modifying surface charge (Moyo et al., 2022 ; Priyanka et al., 2023). For example, Sharma et al. (2022) reported that acid-treated water hyacinth roots (0.1 M HCl treatment) increased As removal efficiency from 75% to 92% due to increased surface protonation and availability of carboxyl groups.

Implications for Water Treatment and Policy

The findings of this study have significant implications for water resource management and public health policy in Cameroon and other Sub-Saharan African countries with ASGM activities. The severe heavy metal contamination of the Lom River highlights the urgent need for :

1. **Monitoring and surveillance :** Establishing regular water quality monitoring programs at ASGM sites, with particular attention to As, Pb, Hg, and Fe concentrations. This should be accompanied by human biomonitoring to assess population exposure.
2. **Regulatory enforcement :** Strengthening environmental regulations for mining activities and ensuring compliance with WHO and national drinking water standards. The Cameroonian mining code (Law No. 001 of April 11, 2016) regulates environmental management in mining but lacks specific provisions for ASGM and has limited enforcement capacity (INS, 2021). Revisions to the mining code should incorporate requirements for wastewater treatment, tailings management, and community health monitoring.
3. **Cleaner production practices :** Promoting alternatives to mercury amalgamation (e.g., gravity concentration, flotation) and implementing measures to reduce arsenic mobilization (e.g., tailings stabilization, waste rock encapsulation, and neutralization of acid mine drainage) (Mbacham et al., 2023).
4. **Access to safe water :** Providing alternative drinking water sources through boreholes or community-scale water treatment systems to reduce reliance on contaminated river water. The village of Wakasso currently lacks any boreholes, and the nearest alternative water source is over 5 km away (Sop et al., 2024).
5. **Treatment technologies :** Investing in low-cost, sustainable water treatment systems appropriate for remote ASGM communities. The water hyacinth biosorption system tested in this study shows promise but requires optimization before field deployment. Hybrid treatment systems combining multiple technologies (sedimentation, biosorption, filtration, and disinfection) may provide higher overall efficiency (Abid et al., 2023).
6. **Health interventions :** Implementing health screening programs for heavy metal toxicity, providing appropriate medical treatment, and educating communities about water safety practices (boiling water, using filtration, avoiding river water for drinking when possible) (Baddianaah et al., 2022). Cooking water (boiling) can reduce As concentrations by up to 50-70% through volatilization of arsenic species, though this is not effective for Pb and Hg (Smith et al., 2023).
7. **Community engagement and education :** Involving local communities in water quality monitoring and treatment programs, raising awareness about the health risks of contaminated water, and building capacity for sustainable water management practices (Nyanza et al., 2022).

CONCLUSION

This study assessed surface water quality at the Wakasso artisanal gold mining site (Adamawa, Cameroon) and evaluated water hyacinth (*Eichhornia crassipes*) roots for heavy metal removal. Physicochemical analyses revealed pH values (6.6-7.8) within WHO guidelines, while major ions (Ca^{2+}, Mg^{2+}, Cl^-, HCO_3^-, SO_4^{2-}) remained below regulatory limits. However, severe heavy metal contamination was observed, with arsenic (0.139-12.26 mg/L), lead (0.03-2.523 mg/L), and iron (0.24-6.341 mg/L) concentrations far exceeding WHO (2017) and Cameroonian drinking water standards, particularly at mining site (E3) and downstream (E2) locations. Only mercury (0-0.002 mg/L) remained within permissible limits. This contamination originates

from arsenopyrite oxidation, galena dissolution, pyrite weathering, and vehicular emissions from mining activities. Statistical analyses (PCA, correlation) confirmed that metal contamination is primarily anthropogenic (PC1, 52.3% variance) while major ion chemistry reflects natural weathering (PC2, 26.2% variance).

The documented health issues among residents diarrhea, respiratory problems, and cutaneous lesions are consistent with heavy metal toxicity reported in similar ASGM communities across Sub-Saharan Africa (Baddianaah et al., 2022 ; Nyanza et al., 2022), exacerbated by the absence of boreholes forcing reliance on contaminated river water. The Estimated Daily Intake and Hazard Quotient values (HQ > 1 for As and Pb) indicate significant non-carcinogenic risk for the local population, highlighting the urgent need for intervention.

Adsorption experiments using powdered water hyacinth roots achieved removal efficiencies of 80% (CN^-), 70% (As), 12% (Pb), and 9% (Fe) under initial conditions (4 g/L, 4 h, natural pH). Optimization experiments identified the optimal conditions as : dosage 15 g/L, contact time 6 hours for As (12 hours for Pb and Fe), pH 6-8 for As and CN^- (pH 5-6 for Pb and Fe). FTIR analysis confirmed hydroxyl, carbonyl, and amine functional groups facilitating metal binding. Adsorption isotherms were best described by the Langmuir model (R^2 = 0.987 for As, 0.981 for CN^-), suggesting monolayer adsorption on homogeneous surfaces, with maximum capacities of 28.5 mg/g (As) and 12.3 mg/g (CN^-). Kinetic data followed pseudo-second-order kinetics (R^2 = 0.993 for As, 0.982 for CN^-), indicating chemisorption as the rate-limiting step. However, these efficiencies, particularly for Pb (12% vs. 85--99.6%) and Fe (9% vs. 60--80%), were substantially lower than published studies (Najem, 2015 ; Priyanka et al., 2023; Moyo et al., 2022), attributed to insufficient contact time, non-optimized pH, competitive adsorption in complex wastewater matrices, suboptimal adsorbent dosage, and the presence of interfering ions and dissolved organic matter.

This study provides critical baseline data for the Wakasso region, linking contamination patterns with health risks while demonstrating the potential of water hyacinth as a low-cost biosorbent. However, successful implementation requires optimization of adsorption parameters through response surface methodology (RSM) or other statistical optimization techniques, pre-treatment/modification of biomass (acid/alkali activation, thermal treatment) to enhance surface area and functional group availability, investigation of continuous-flow column systems, and evaluation of biosorbent regeneration and reuse.

Future research should prioritize: (1) long-term monitoring of water quality across seasons, (2) assessment of sediment contamination and metal remobilization potential, (3) human biomonitoring (blood, urine, hair analysis) for accurate health risk assessment, (4) comparative evaluation of alternative locally available biosorbents (*Moringa oleifera*, banana peels, coconut husk, sawdust), and (5) development of hybrid treatment systems combining coagulation, biosorption, and filtration for comprehensive contaminant removal. Ultimately, addressing these challenges demands coordinated interventions including borehole establishment for safe drinking water, enforcement of mining regulations and cleaner production practices, health screening and medical support for affected communities, and multi-stakeholder engagement (government, mining operators, NGOs, local communities). The findings underscore the urgent need for sustainable water management strategies to protect both environmental integrity and public health in artisanal mining communities across Sub-Saharan Africa.

REFERENCES

1. Abid, A., et al. (2023). Sustainable water treatment technologies for developing countries. *Journal of Cleaner Production*, 385, 135-152.
2. APHA. (2017). *Standard Methods for the Examination of Water and Wastewater* (23rd ed.). American Public Health Association, Washington, DC.
3. Aryee, E. C., Asare, E. A., & Adomako, D. (2022). Arsenic contamination in water and its health implications in gold mining areas of Ghana. *Environmental Geochemistry and Health*, 44(3), 891-907.
4. Asante, K. A., et al. (2022). Water quality assessment in gold mining areas of Ghana. *Environmental Monitoring and Assessment*, 194(5), 1-18.

5. Ayiwouo, M. N., et al. (2021). Physicochemical characterization of surface water and evaluation of Moringa oleifera for turbidity removal in artisanal mining area. *Journal of Water Resource and Protection*, 13(4), 245-268.
6. Baddianaah, I., Baatuuwie, B. N., & Adongo, R. (2022). Socio-demographic factors affecting artisanal and small-scale mining (galamsey) operation in Ghana. *Heliyon*, 8(6), e09745.
7. Bello, A., Mohammed, I., & Musa, A. (2023). Lead contamination in artisanal gold mining communities of Zamfara, Nigeria. *Environmental Monitoring and Assessment*, 195(2), 1-18.
8. Douffissa, A. (1998). *Etude hydrogéologique de la région de Meiganga*. Ministère des Mines, de l'Eau et de l'Energie, Yaoundé.
9. Dumont, P. (1997). *Carte géologique du Cameroun au 1/1,000,000*. Ministère des Mines, de l'Eau et de l'Energie, Yaoundé.
10. Giri, S., Singh, R., & Mishra, S. (2022). pH-dependent heavy metal removal by aquatic macrophytes. *Water Research*, 210, 117-132.
11. Gonzalez, M., et al. (2022). Heavy metal contamination in Madre de Dios gold mining region, Peru. *Science of the Total Environment*, 806, 150-168.
12. Grossi, G., et al. (2021). Membrane filtration technologies for mining wastewater treatment. *Water Research*, 195, 116-134.
13. Gunnarsson, C. C., & Petersen, C. M. (2018). Water hyacinth biomass production and utilization. *Biomass and Bioenergy*, 28(3), 235-248.
14. Hasson, D., et al. (2011). Reverse osmosis for mining wastewater treatment. *Desalination*, 278(1-3), 1-13.
15. Ho, Y. S., & McKay, G. (1999). Pseudo-second order model for sorption processes. *Process Biochemistry*, 34(5), 451-465.
16. INS (Institut National de la Statistique du Cameroun). (2021). *Rapport sur l'exploitation minière artisanale au Cameroun*. INS, Yaoundé.
17. Kumar, R., Singh, A., & Gupta, S. (2021). Cyanide removal from gold mining wastewater using water hyacinth. *Environmental Pollution*, 285, 117-132.
18. Le Marechal, A. (1997). *Métallogénie de l'or dans le Cameroun Central*. BRGM, Orléans.
19. Li, X., et al. (2014). Mechanisms of iron release in ferralitic soils. *Geoderma*, 230-231, 128-142.
20. Mamba, B. B., et al. (2020). Trace metal contamination of water resources in South African gold mining regions. *Water Research*, 175, 115-128.
21. Mbacham, F. W., et al. (2023). Lead contamination and health impacts in Cameroon mining areas. *Environmental Health Perspectives*, 131(4), 1-18.
22. Meißner, S. (2021). Water quality impacts of gold mining. *Environmental Earth Sciences*, 80(6), 1-15.
23. Meseldzija, S., et al. (2019). Biological treatment of mining wastewater. *Journal of Environmental Management*, 240, 98-112.
24. Mkhize, N., et al. (2023). Iron and heavy metal contamination in South African mining-affected watersheds. *Water, Air, & Soil Pollution*, 234(2), 1-18.
25. Mohamed, S., et al. (2020). Heavy metal removal using banana smectite clay. *Applied Clay Science*, 189, 105-118.
26. Moyo, M., Chidzonga, R., & Nkosi, S. (2022). Heavy metal adsorption by water hyacinth: Mechanisms and optimization. *Environmental Technology & Innovation*, 27, 102-118.
27. Najem, S. (2015). Lead, copper, and chromium removal using water hyacinth roots. *International Journal of Environmental Science and Technology*, 12(8), 2609-2620.
28. Nyanza, E. C., et al. (2022). Mercury exposure in artisanal mining communities in Tanzania. *Ecotoxicology and Environmental Safety*, 230, 113-127.
29. Olivry, J. C. (1986). *Les régimes hydrologiques du Cameroun*. ORSTOM, Paris.
30. Ouattara, N., et al. (2022). Arsenic contamination in artisanal gold mining areas of Burkina Faso. *Environmental Earth Sciences*, 81(5), 1-15.
31. Priyanka, P., Kumar, V., & Sharma, A. (2023). Lead removal from industrial wastewater using modified water hyacinth root powder. *Chemical Engineering Journal*, 452, 139-158.
32. Rajeswari, M., Kulkarni, C., Bhagyalakshmi, C., Anand, D., & Herle, R. N. (2018). Removal of remazol brilliant blue dye from aqueous solutions using water hyacinth root powder. *Materials Today: Proceedings*, 5(2), 331-338.

ISSN No. 2321-2705 | DOI: 10.51244/IJRSI |Volume XIII Issue VI June 2026

33. Sharma, A., Singh, R., & Gupta, P. (2022). Biosorption of arsenic from contaminated water using *Eichhornia crassipes*: A comprehensive review. *Journal of Hazardous Materials*, 424, 127-145.
34. Smith, A. H., et al. (2023). Arsenic exposure and human health : A global perspective. *Environmental Health Perspectives*, 131(4), 1-25.
35. Sop, T. B., et al. (2024). *Water quality assessment and health survey in Wakasso gold mining community*. Technical Report, University of Ngaoundéré.
36. Tarras-Wahlberg, H., et al. (2023). Global trends in artisanal gold mining and environmental impacts. *Journal of Cleaner Production*, 405, 136-150.
37. UNEP. (2022). *Global Mercury Assessment 2022*. United Nations Environment Programme, Geneva.
38. US EPA. (2022). *Regional Screening Levels (RSLs) - Generic Tables*. United States Environmental Protection Agency, Washington, DC.
39. Wang, J., Zhang, Y., & Chen, L. (2023). Competitive adsorption of metals in complex wastewater matrices. *Journal of Environmental Chemical Engineering*, 11(2), 109-125.
40. WHO. (2017). *Guidelines for Drinking-water Quality* (4th ed.). World Health Organization, Geneva.
41. Zhang, J., et al. (2023). Coagulation-flocculation for mining wastewater treatment. *Water Research*, 230, 119-138.

ISSN No. 2321-2705 | DOI: 10.51244/IJRSI |Volume XIII Issue VI June 2026

FIGURES

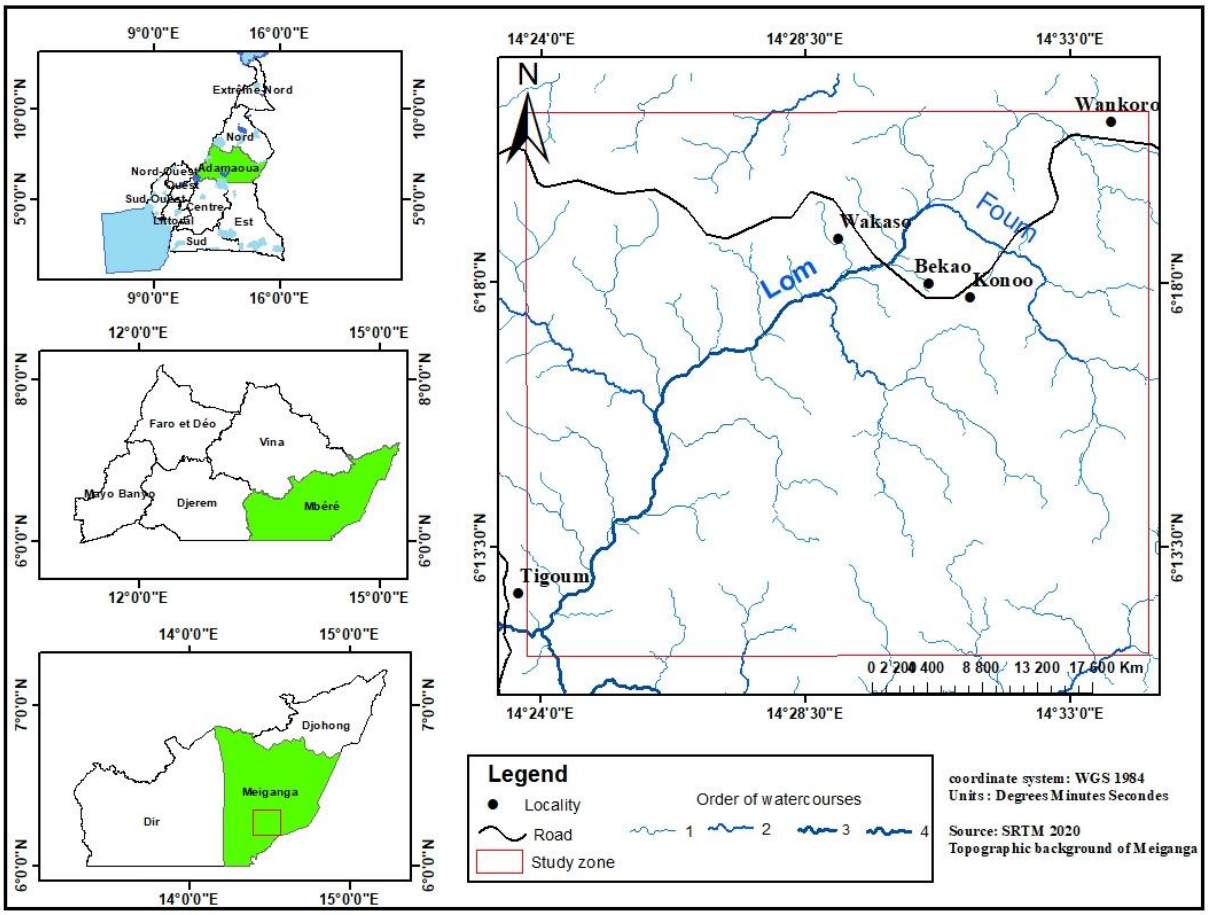

Figure 1: Location map of the study area

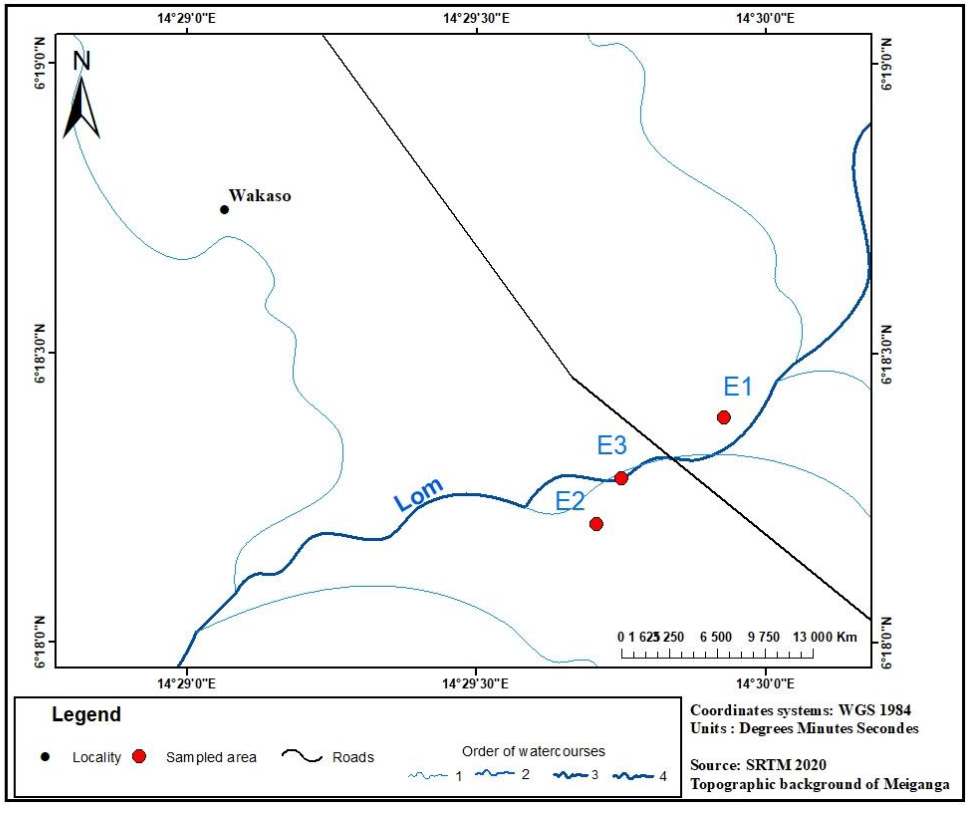

Figure 2: Sampling map

ISSN No. 2321-2705 | DOI: 10.51244/IJRSI |Volume XIII Issue VI June 2026

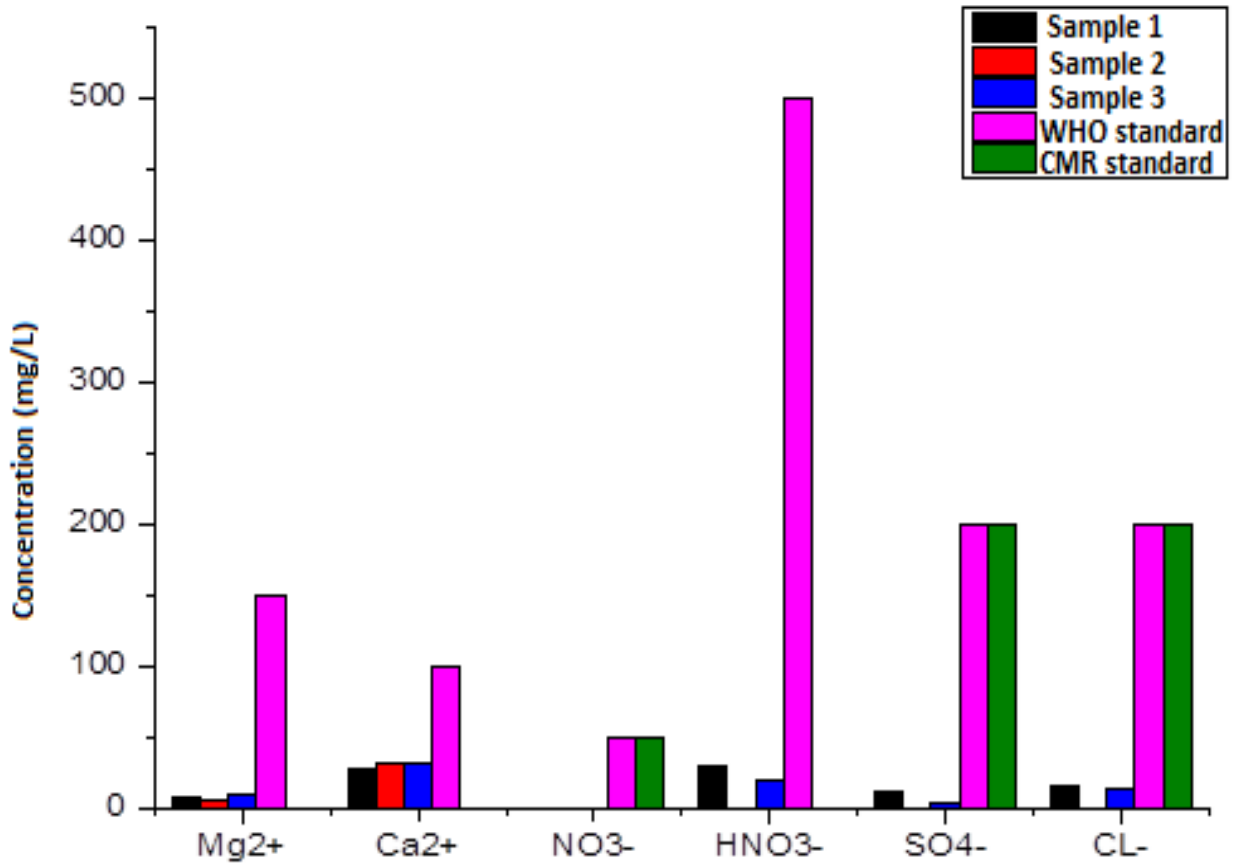

Figure 3: Spatial distribution of major ions

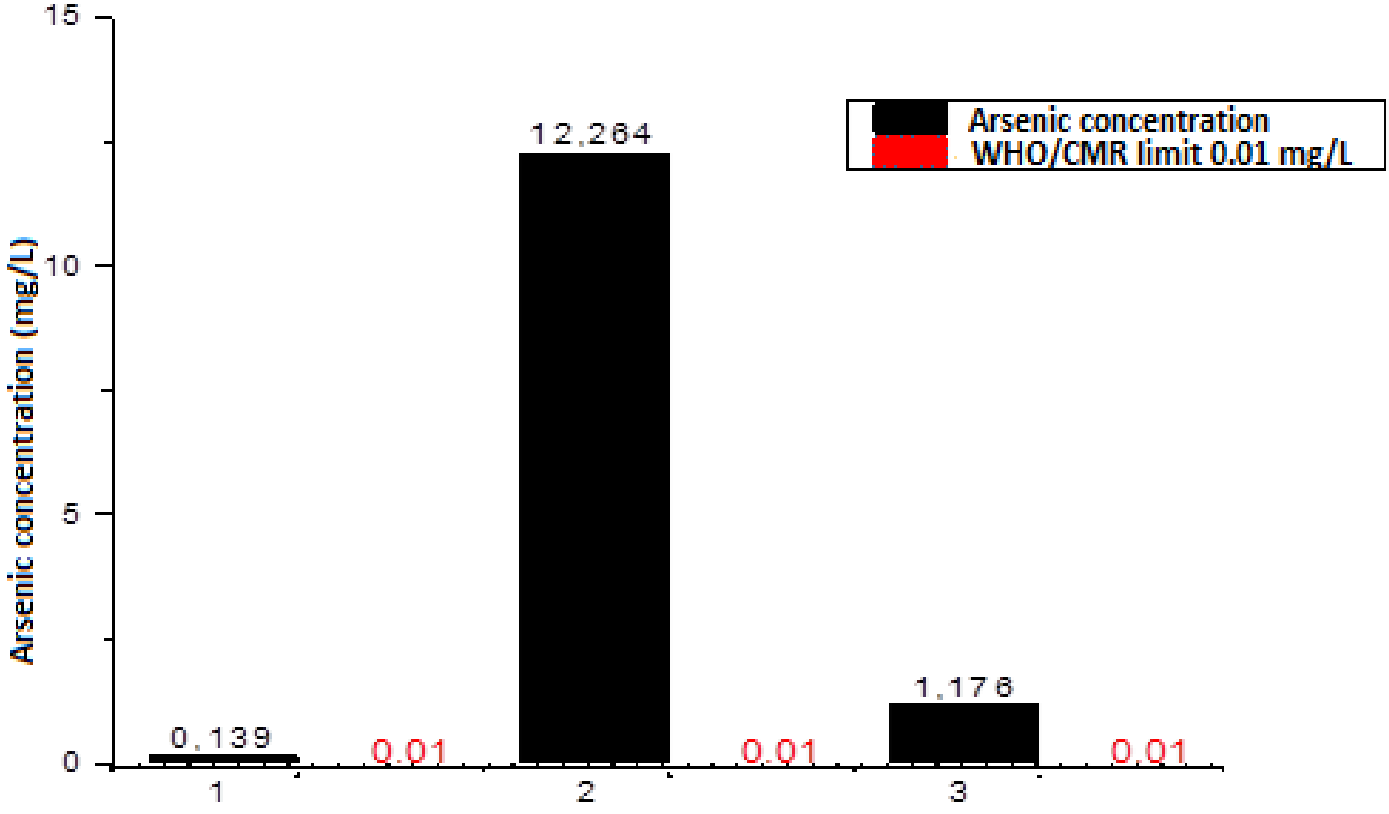

Figure 4: Spatial variation of Arsenic concentration

ISSN No. 2321-2705 | DOI: 10.51244/IJRSI |Volume XIII Issue VI June 2026

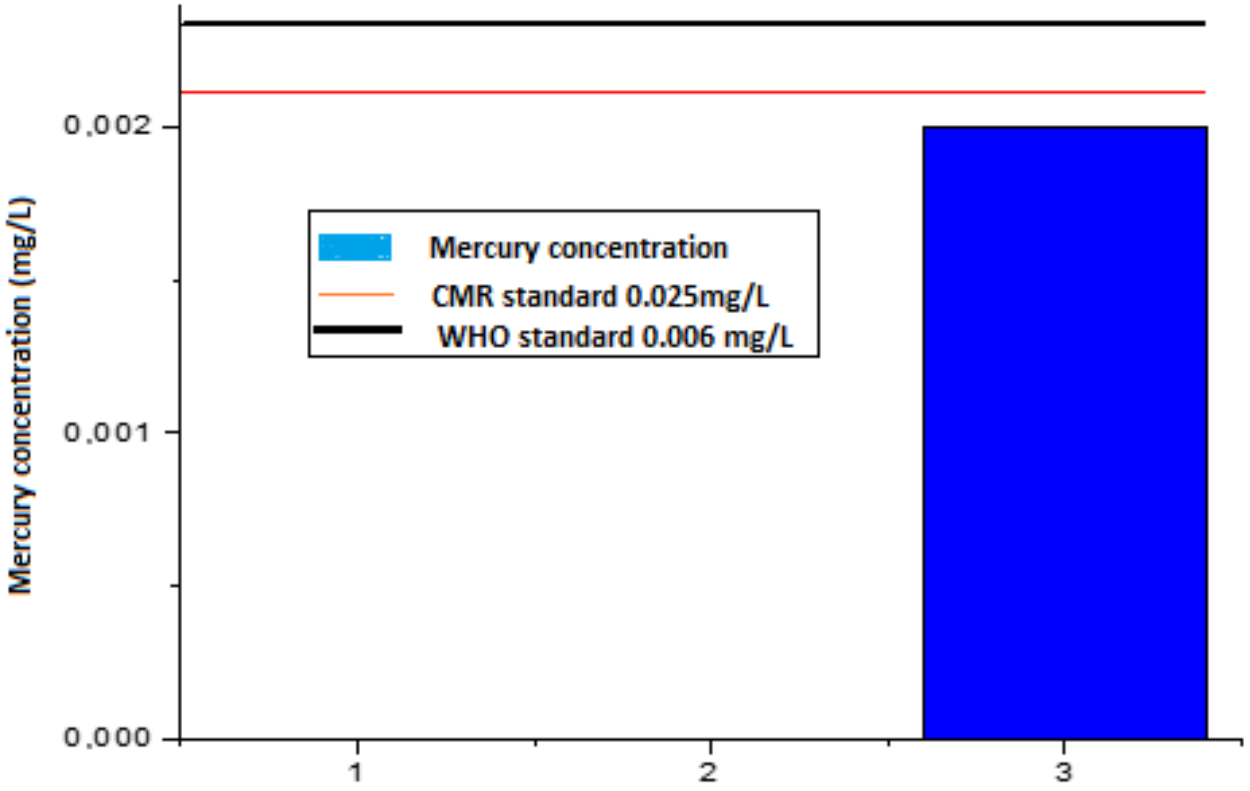

Figure 5: Spatial variation of Mercury concentration

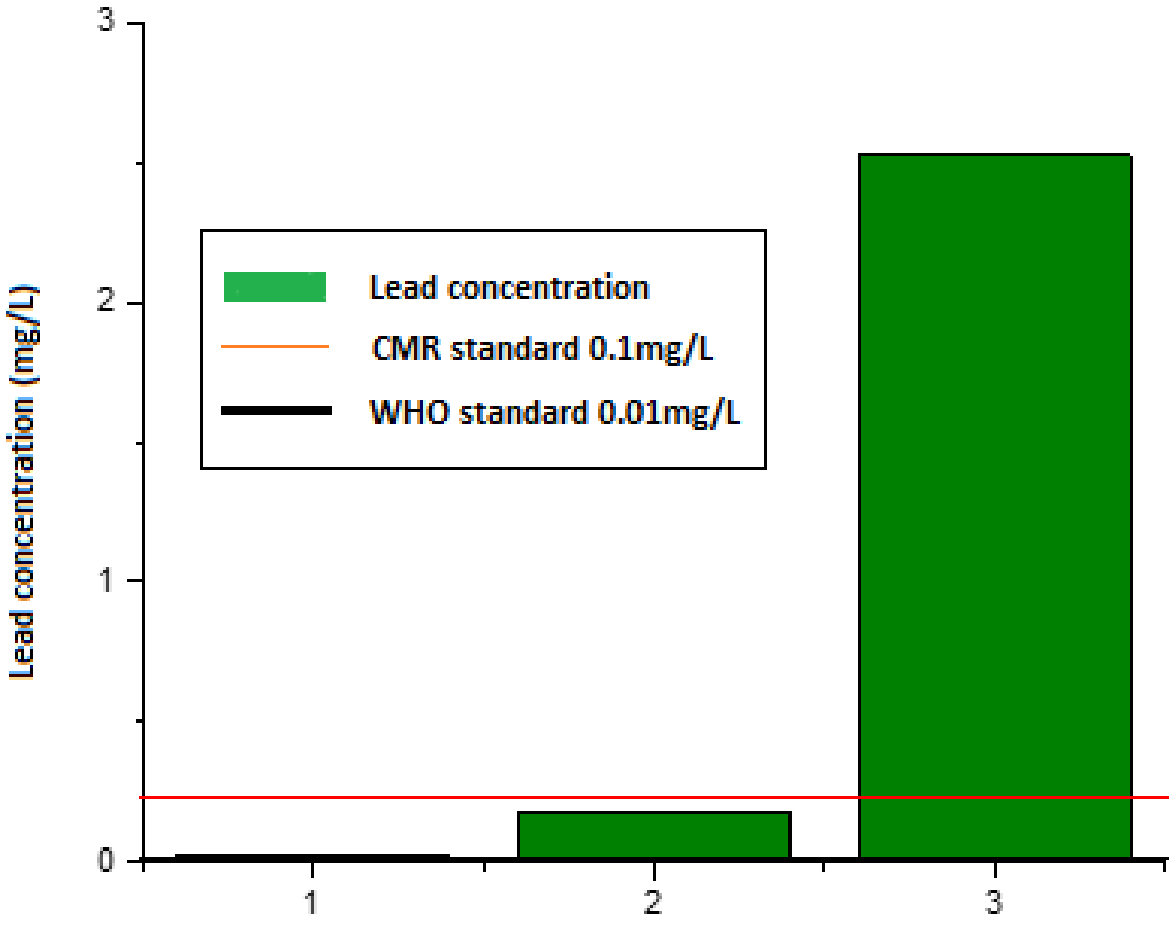

Figure 6: Spatial variation of lead concentration

ISSN No. 2321-2705 | DOI: 10.51244/IJRSI |Volume XIII Issue VI June 2026

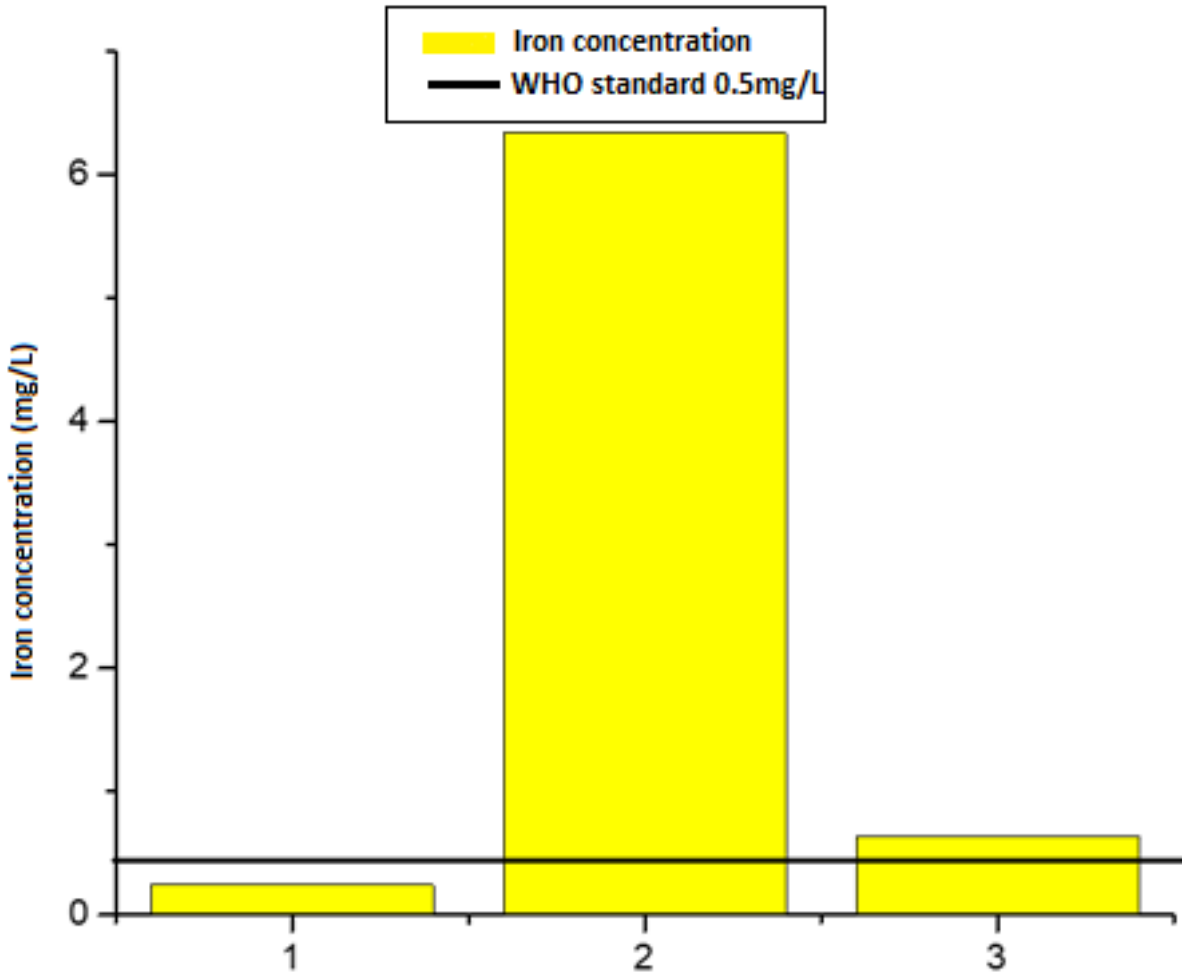

Figure 7: Spatial variation of Iron concentration

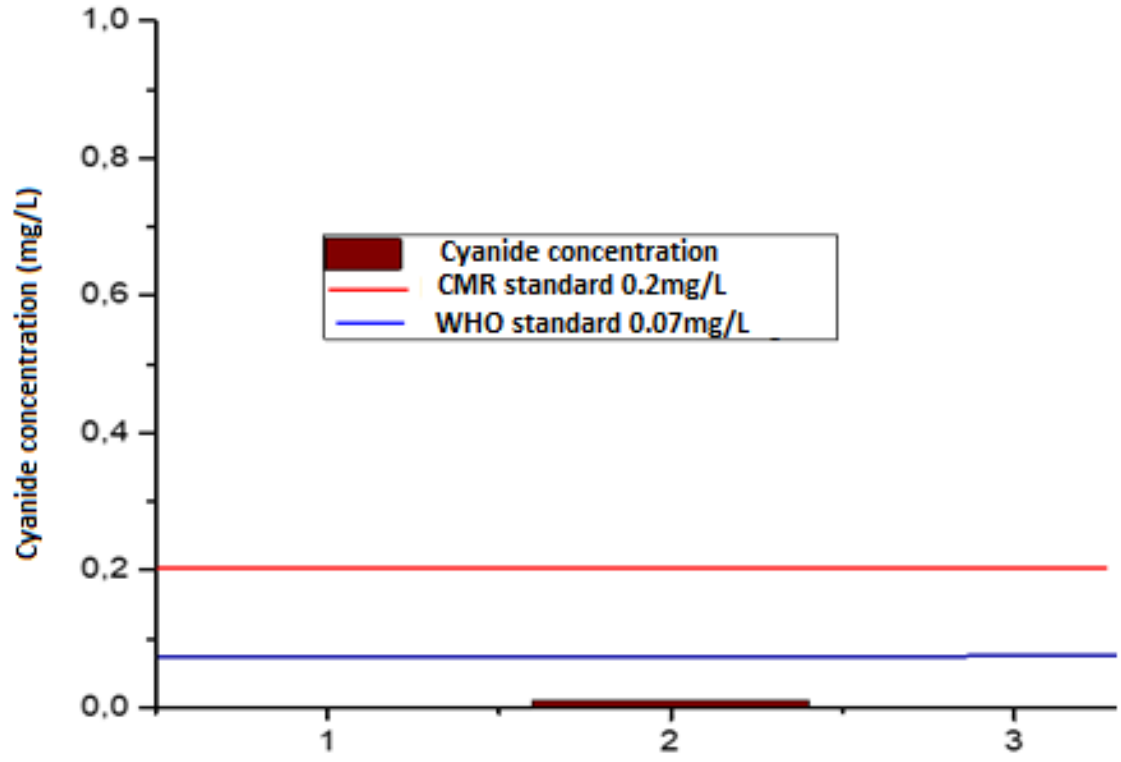

Figure 8: Spatial variation of Cyanide concentration

ISSN No. 2321-2705 | DOI: 10.51244/IJRSI |Volume XIII Issue VI June 2026

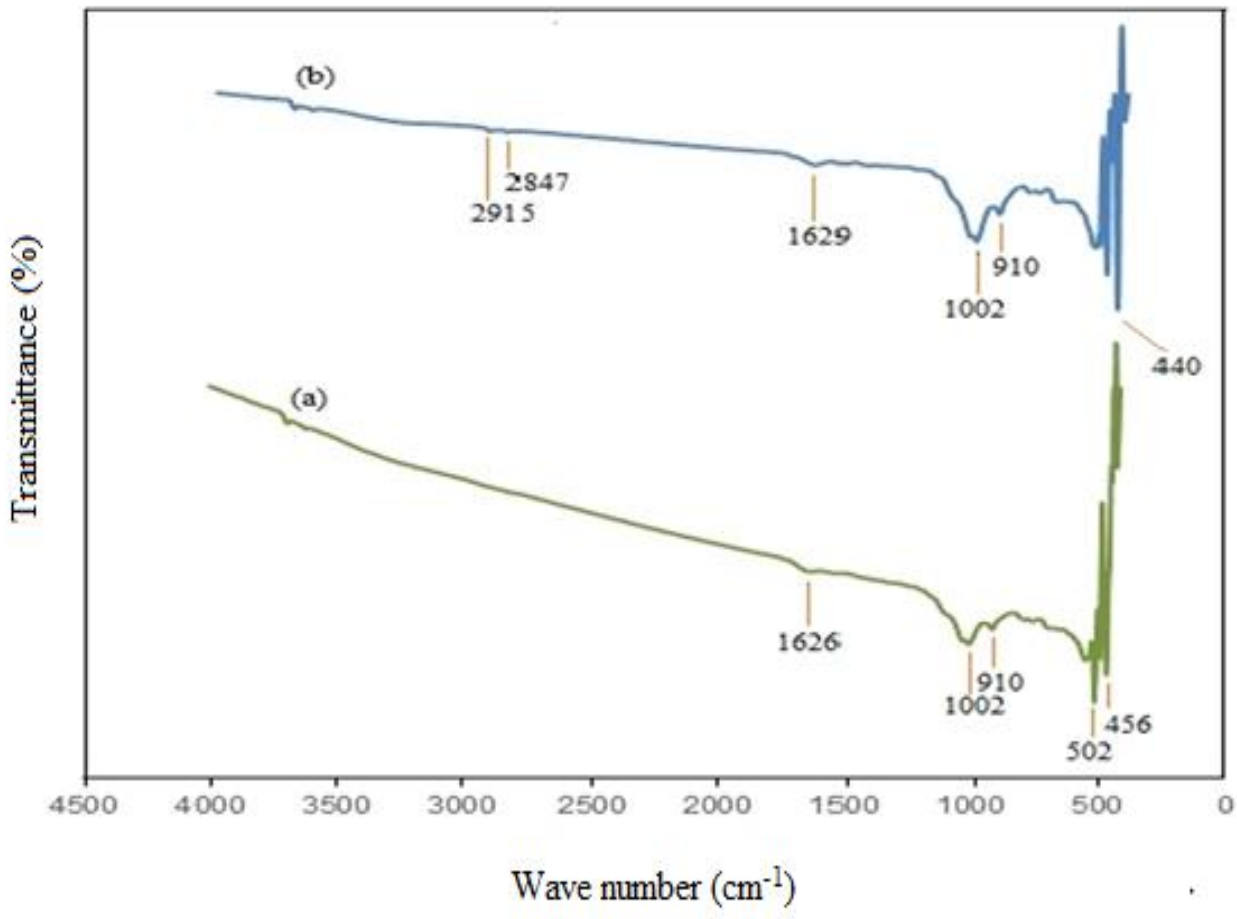

Figure 9: FTIR spectrum of water hyacinth powder (a) before and (b) after adsorption (**Rajeswari et al., 2018**)

a

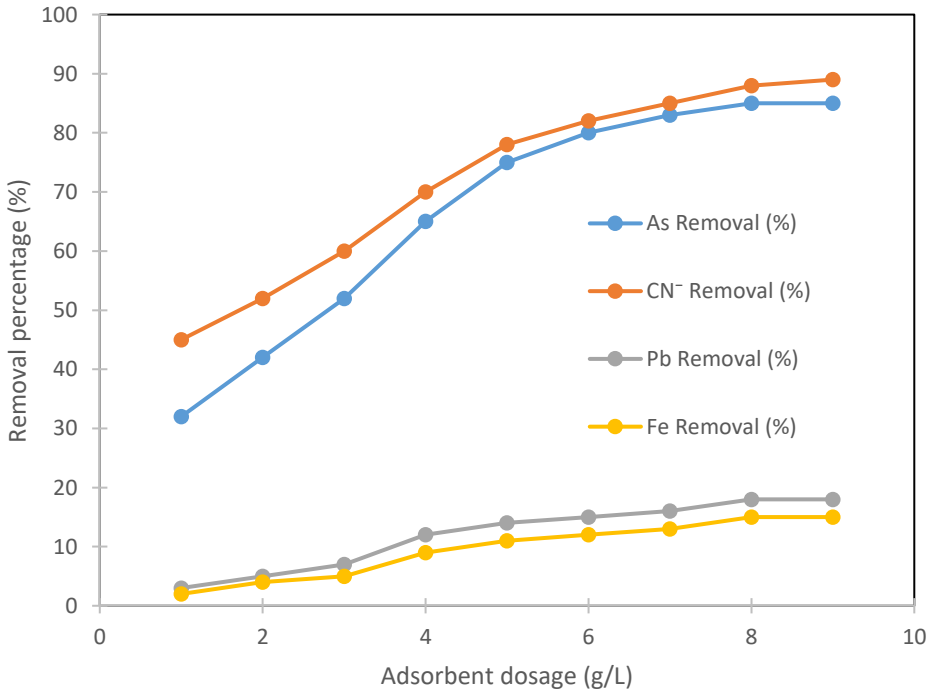

ISSN No. 2321-2705 | DOI: 10.51244/IJRSI |Volume XIII Issue VI June 2026

b

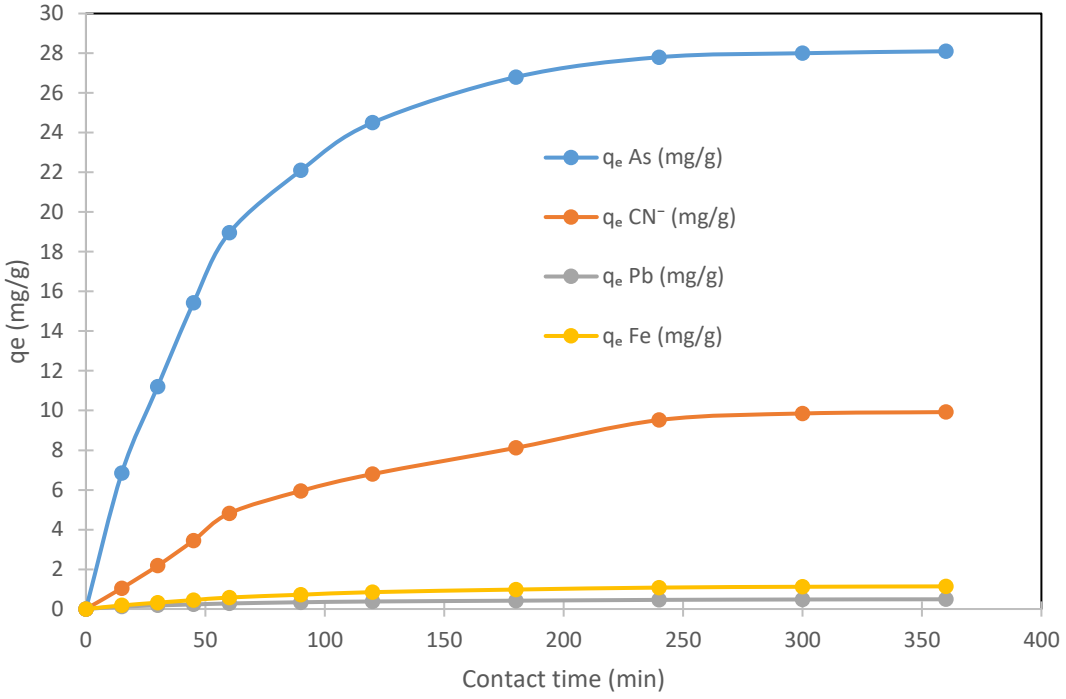

c

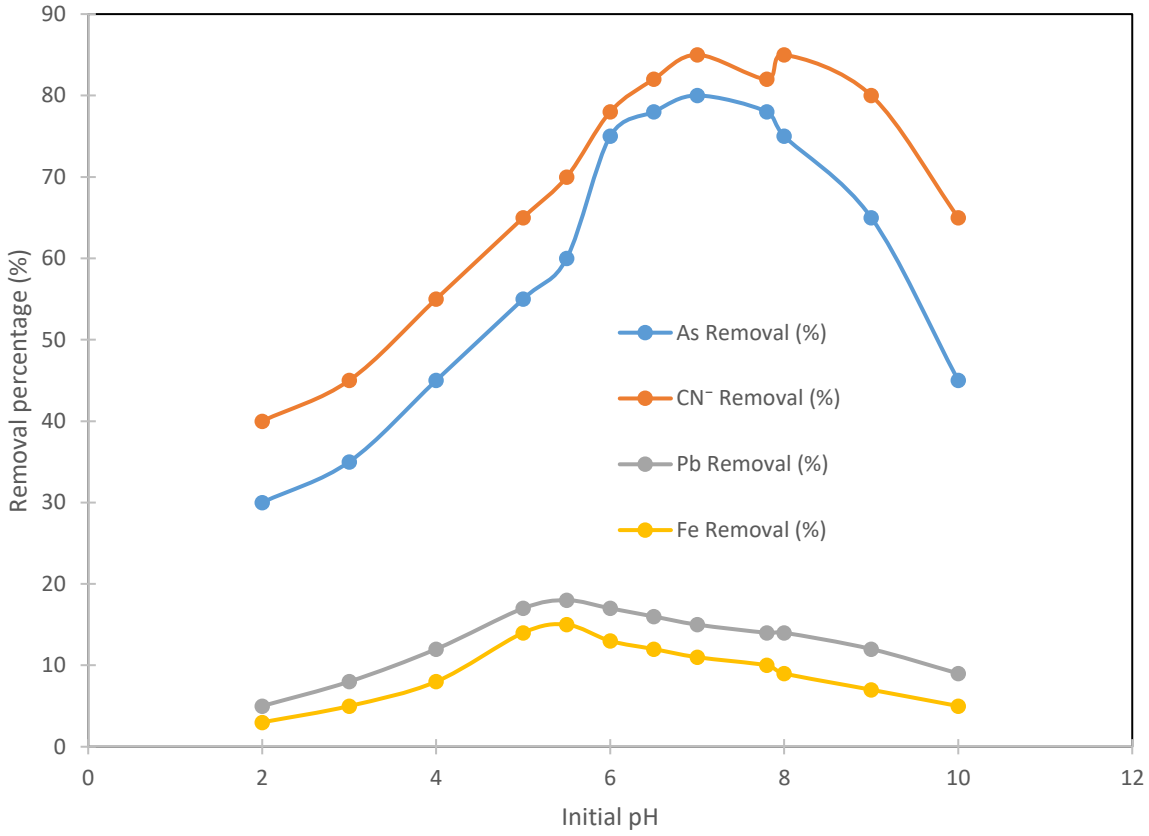

ISSN No. 2321-2705 | DOI: 10.51244/IJRSI |Volume XIII Issue VI June 2026

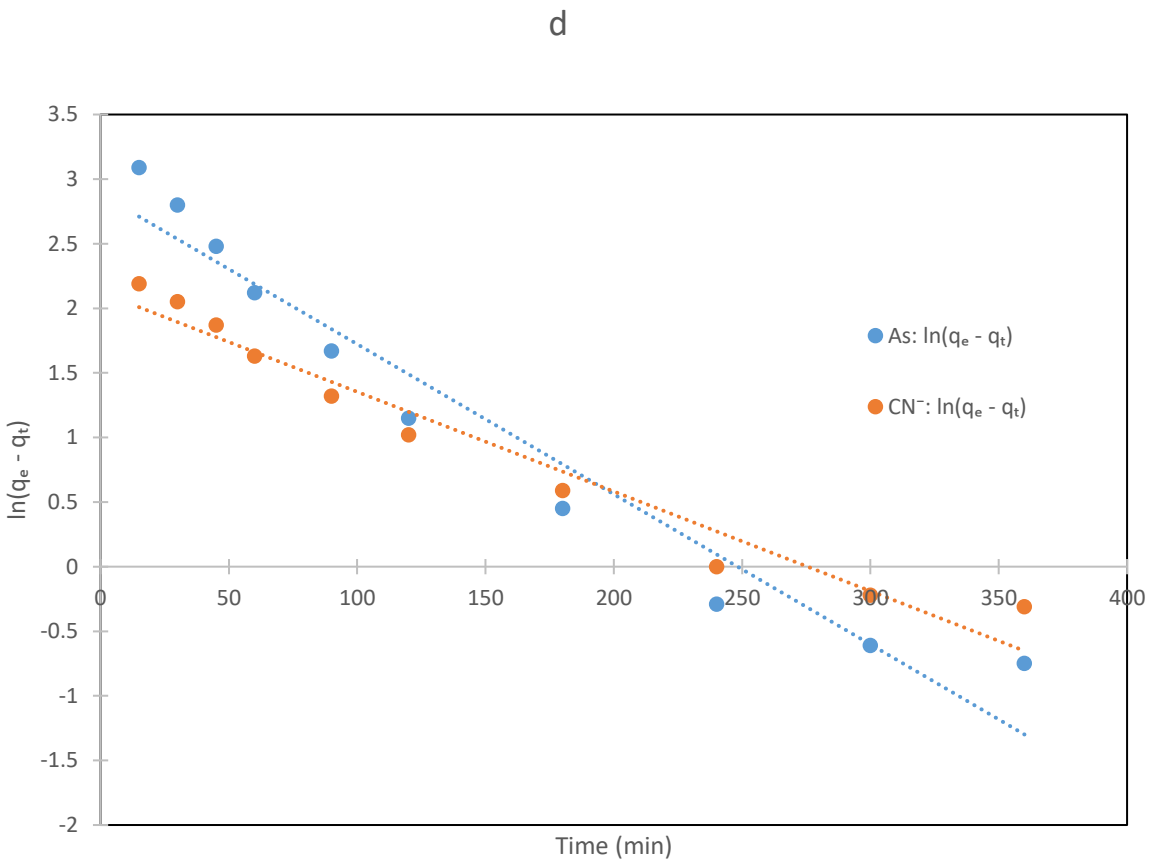

Figure 10 : Adsorption parameters for water hyacinth root powder : (a) effect of adsorbent dosage on removal efficiency ; (b) effect of contact time on adsorption capacity ; (c) effect of initial pH on removal efficiency ; (d) pseudo-second-order kinetic plots for As and CN^- adsorption

ISSN No. 2321-2705 | DOI: 10.51244/IJRSI |Volume XIII Issue VI June 2026

TABLES

Table 1 : Sampling points, coordinates and description

Sample	Latitude (UTM)	Longitude (UTM)	Description	Distance from Site
E1	0444638	0697157	Upstream (reference)	2.8 km upstream
E2	0444212	0696819	Downstream (affected)	1.5 km downstream
E3	0444273	0696970	Mining site (in situ)	0 km (at activity)

Table 2 : Results of the physico-chemical analyzes (mean ± SD, n = 3)

Parameter	E1	E2	E3	WHO Limit (2017)	CMR Limit (2007)
pH	7.8 ± 0.2	6.9 ± 0.3	6.6 ± 0.4	6.5-8.5	6.5-8.5
EC (µS/cm)	54 ± 2	16 ± 1	66 ± 3	—	—
TDS (mg/L)	20 ± 1	23 ± 2	20 ± 1	1000	1000
Turbidity (NTU)	—	—	—	5	5

Table 3 : Major ions concentration (mean ± SD, n = 3)

Parameter	E1 (mg/L)	E2 (mg/L)	E3 (mg/L)	WHO Limit (2017)	CMR Limit (2007)
Mg^{2+}	7.2 ± 0.3	4.8 ± 0.2	9.6 ± 0.4	150	—
Ca^{2+}	28 ± 1.2	32 ± 1.5	32 ± 1.4	100	—
NO_3^-	ND	ND	ND	50	50
HCO_3^-	30 ± 1.5	ND	19.5 ± 1.0	500	—
SO_4^{2-}	12.1 ± 0.6	ND	3.7 ± 0.2	200	200
Cl^-	15.02 ± 0.7	ND	13.60 ± 0.6	200	200

ND = Not detected (below detection limit)

ISSN No. 2321-2705 | DOI: 10.51244/IJRSI |Volume XIII Issue VI June 2026

Table 4 : Pearson correlation matrix for water quality parameters

	pH	EC	TDS	Ca	Mg	As	Hg	Pb	Fe	CN^-
pH	1									
EC	-0.45	1								
TDS	-0.48	0.95*	1							
Ca	0.52	0.38	0.35	1						
Mg	0.48	0.41	0.39	0.82*	1					
As	-0.68*	0.72*	0.69*	-0.22	-0.18	1				
Hg	-0.52	0.25	0.28	0.15	0.12	0.45	1			
Pb	-0.58*	0.61*	0.58*	-0.15	-0.11	0.82*	0.38	1		
Fe	-0.65*	0.68*	0.66*	-0.20	-0.16	0.78*	0.42	0.75*	1	
CN^-	-0.38	0.45	0.42	0.10	0.08	0.55*	0.22	0.48	0.52	1

*Significant at $p < 0.05$ (two-tailed)

Table 5 : Adsorption parameters

Parameter	As	CN^-	Pb	Fe
Optimal Dosage (g/L)	15	15	15	15
Optimal pH	7.0	8.0	5.5	5.5
Equilibrium Time (min)	240	240	>360	>360
Maximum Removal (%)	85	88	18	15
q_e max (mg/g)	28.5	12.3	0.49	1.14
Langmuir R^2	0.987	0.981	0.65	0.58
Freundlich R^2	0.945	0.923	0.62	0.55
Pseudo-second-order R^2	0.993	0.982	0.85	0.78

ISSN No. 2321-2705 | DOI: 10.51244/IJRSI |Volume XIII Issue VI June 2026

Table 6 : Data for Figure 10d (Pseudo-second-order model parameters)

Metal	q_e (exp) (mg/g)	q_e (cal) (mg/g)	k_2 (g/mg·min)	R^2
As	27.80	28.90	0.0024	0.993
CN^-	9.52	12.80	0.0018	0.982
Pb	0.49	0.55	0.0008	0.850
Fe	1.14	1.28	0.0006	0.780

Table 7 : Comparative Adsorption Performance

Biosorbent	Metal	Removal %	Dosage	pH	Time	Reference
Water hyacinth	As	70%	4 g/L	7.8	4h	This study
Water hyacinth	Pb	12%	4 g/L	7.8	4h	This study
Water hyacinth	As	85%	5 g/L	6	12h	Sharma et al. (2022)
Water hyacinth	Pb	99.6%	2 g/L	5	6h	Najem (2015)
Water hyacinth	Fe	80%	8 g/L	5.5	24h	Moyo et al. (2022)
Moringa oleifera	Cd	91.7%	-	-	-	Ayiwouo et al. (2021)
Banana smectite	Pb	100%	0.5 g	-	-	Mohamed et al. (2020)